NANO LETTERS

2009
Vol. 9, No. 4
1369-1373

Negative Differential Resistance: Gate Controlled and Photoconductance Enhancement in Carbon Nanotube Intraconnects

S. W. Lee,[†] A. Kornblit,[‡] D. Lopez,[‡] S. V. Rotkin,[§] A. A. Sirenko,[||] and H. Grebel*,[†]

Electronic Imaging Center at NJIT, Department of Electrical and Computer Engineering, Department of Physics, New Jersey Institute of Technology, Newark, New Jersey 07102, New Jersey Nanotechnology Consortium (NJNC), Alcatel-Lucent Technologies Bell Laboratories, Murray Hill, New Jersey 07974, and Physics Department and Center for Advance Materials and Nanotechnology, Lehigh University, Bethlehem, Pennsylvania 18015

Received October 6, 2008; Revised Manuscript Received January 12, 2009

ABSTRACT

Intraconnects, as-grown single-walled carbon nanotubes bridging two metal electrodes, were investigated as gated structures. We show that even with a seemingly "ohmic" contact at zero gate voltage one observes negative differential resistance (NDR) at nonzero gate bias. Large differential photo conductance (DPC) was associated with the NDR effect raising hopes for the fabrication of novel high-speed optoelectronic devices.

Single-wall carbon nanotube (SWCNT) intraconnects (bridges spanning across two planar electrodes (Figure 1) have gained large attention from basic research and application[1−11] points of view. Several investigations have been devoted to the theoretical[12−14] and experimental[15−20] aspects of the contact between the bridging tube(s) and metal. By comparison, fewer studies were devoted to a related negative differential resistance (NDR) effect, which is important for the construction of high-frequency oscillators. In the past, we have devised a way of fabricating SWCNT intraconnects at high yield; sharp electrode tips were used as seed catalysts thus, initiating the tube's growth from tip to tip. We used this method to study the characteristics of gated structures with channels made of individual or small number of bundled tubes. Such electrode construction enabled us to interrogate intraconnects by Raman spectroscopy, current−voltage characteristics and their response to white light irradiation. As we shall see below, the intraconnects exhibited NDR, which was associated with a large differential photo conductance for both ohmic and nonohmic contacts (defined at zero gate bias).

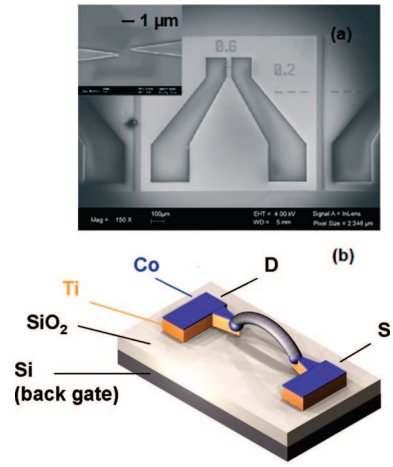

Figure 1. (a) SEM image of the metal electrodes. The distance between two sharp tips was 1 μm. Individually addressable CNT intraconnect was grown directly from tip to tip by CVD. (b) Schematic diagram of our CNT FET. Co was deposited as a catalyst on top of Ti electrode to initiate CNT intraconnect growth. Si substrate was used as a back gate.

Experiments and Methods. SWCNT intraconnects were grown and self-aligned between prefabricated electrodes by use of chemical vapor deposition (CVD).[21,22] For the present

* To whom correspondence should be addressed. E-mail: grebel@njit.edu. Tel: 1-973-596-3538.
[†] Electronic Imaging Center at NJIT and the Department of Electrical and Computer Engineering, New Jersey Institute of Technology.
[‡] Alcatel-Lucent Technologies Bell Laboratories.
[§] Lehigh University.
[||] Department of Physics, New Jersey Institute of Technology.

10.1021/nl803036a CCC: $40.75
Published on Web 03/02/2009

study we replaced the CO precursor gas with methane/hydrogen mixture at elevated temperatures.[23] While some of the intraconnects could not be observed by scanning electron microscope (SEM), nonetheless they had a clear current−voltage ($I-V$) and Raman scattering characteristics. The electrode construction and labeling made it easy to assess the tubes even one year after fabrication. We made sure that nonmetalized surfaces, away from the electrode region, did not contribute to the electrical path. In addition, the electrode shape enabled focusing of the laser beam, used for Raman spectroscopy, right in-between the electrodes (see Supporting Information). All electrical and optical measurements were performed at room temperature.

Figure 1 shows an SEM image of the electrodes. Here, the distance between the two electrode tips was 1 μm, though the electrode layout had coaligned and laterally shifted patterns (Figure 1a inset). The schematic of a gated structure, made of CNT intraconnect, is shown in Figure 1b. The two metal electrodes were used as source and drain electrodes, respectively. A silicon substrate was used as a back gate electrode. The silicon surface was oxidized to a thickness of 20 nm prior to the electrode deposition.

Raman spectra were measured using the 514.5 nm line of an ion Ar^+ laser, a single grating spectrometer, which was equipped with two notch filters for laser line rejection and a N_2 cooled CCD detector. The system was equipped with a $\times 50$ microscope to aid focusing of the laser light between the sharp tips of the electrodes. The Raman spectra of SiO_2 and Si away from the bridge were used as reference and were subtracted from the spectra of the CNT intraconnect. Broadband light illumination was made with a white-light tungsten source, which had a high energy cutoff at 3 eV. The white-light source intensity was 0.25 mW/cm^2, and it was illuminating the entire structure.

Results. Figure 2 shows two examples, one exhibiting nonlinear and the other linear electrical characteristics. Figure 2a−c shows SEM, $I_{ds}-V_{ds}$, and Raman spectra of Sample 1. The nonlinear $I-V$ curve at zero gate voltage indicates a presence of potential barrier between the tube and metal contact(s). The asymmetry in the curve points to one dominant barrier (otherwise, the curve would have been symmetric). Its Raman spectra are shown in Figure 2c. The low frequency spectra exhibit a narrow single peak (5 cm^{-1} wide and limited only by the system resolution) for the radial breathing mode (RBM) at 191.9 cm^{-1}. The peak may indicate a metallic tube (12,6) with an average diameter of 1.252 nm.[24] It exhibits a very large graphitic line at 1355 cm^{-1}, which may indicate defects or, large stress. The high-frequency region exhibits two peaks at 1594 and 1567 cm^{-1}, respectively. Their frequency difference 27 cm^{-1} corresponds to a tube diameter $d = 1.716$ nm if we follow[25] and assume a metallic type tube. It corresponds to a tube diameter $d = 1.329$ nm assuming semiconductor type. Sample 2 exhibits linear $I-V$ characteristics at zero gate bias (Figure 2e). Its low frequency Raman spectrum consists of a broader single RBM peak (30 cm^{-1} wide) centered at 176.2 cm^{-1}, which implies semiconductor tube(s) (11,9) with an average diameter of 1.365 nm. It exhibits a large defect line at 1352 cm^{-1}.

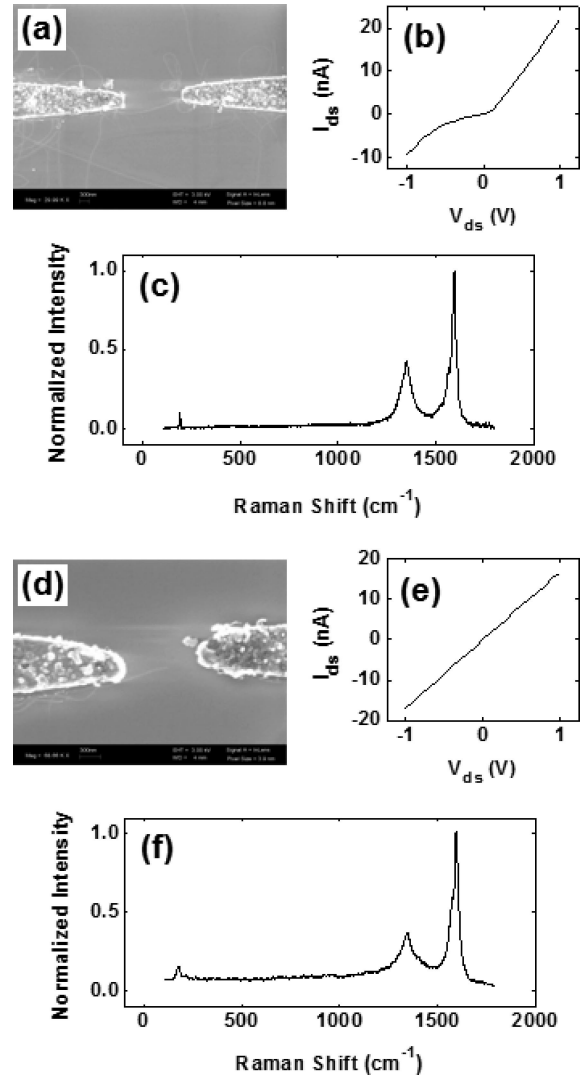

Figure 2. Sample 1: (a) SEM image of CNT intraconnect; (b) nonlinear $I_{ds}-V_{ds}$ characteristic; (c) Raman spectra with RBM at 191.9 cm^{-1}. Sample 2: (d) SEM image of CNT intraconnect; (e) linear $I_{ds}-V_{ds}$ characteristic; (f) Raman spectra with RBM at 176.2 cm^{-1}.

The high-frequency frequency exhibits two peaks at 1596 and 1578 cm^{-1}, respectively. Their difference 18 cm^{-1} implying tube diameters $d = 2.101$ nm and $d = 1.628$ nm for metallic or semiconductor type tubes, respectively.

Electrical properties in the dark and under white light illumination were measured for Sample 1 (Figure 3) and Sample 2 (Figure 4). The channel formed by the intraconnects exhibited a natural p-type characteristics owing to the presence of oxygen in the tubes. Figure 3a shows a map of V_{gs} vs V_{ds} for the nonilluminated intraconnect. Two negative differential resistance (NDR) regions may be observed in the $I_{ds}-V_{gs}$ plot: one, in the range between −3 and −6 V and the other, around −9 V (Figure 3b-c). The NDR peak for the first region was shifting to the negative side as the V_{ds} value increased from 0.25 to 0.75 V (Figure 3c). The second NDR region was stable around −9 V. Characteristics of the same intraconnect under illumination are shown in Figure 3d-f. Surprisingly, the light did not mask the NDR effect (Figure 3f) but locked it to the same V_{gs} range for all

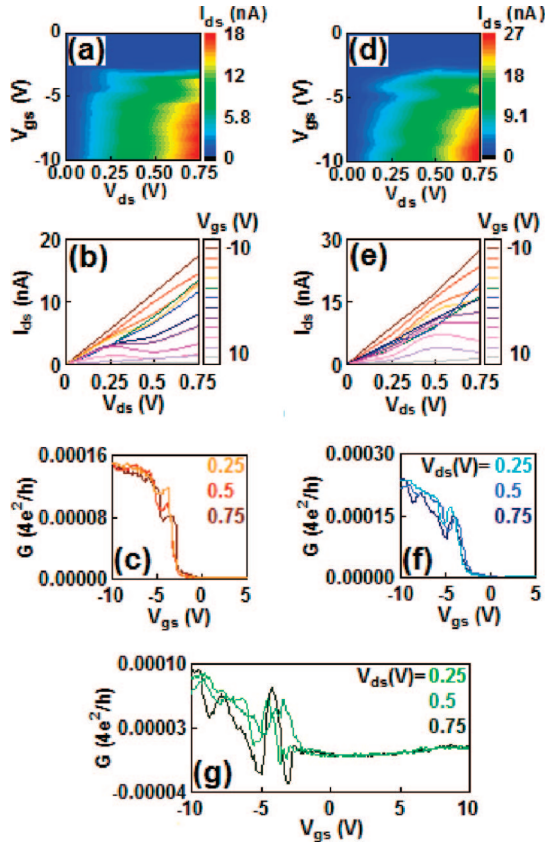

Figure 3. Electrical properties of Sample 1 before and after white light illumination. (a) I_{ds} vs V_{gs} and V_{ds} characteristics. Negative differential resistance was observed for V_{gs} between −2 and −6. (b) $I_{ds}-V_{ds}$ characteristic for various V_{gs} values from +10 to −10. $I_{ds}-V_{ds}$ curves become nonlinear when the gate voltages for a negative differential region are applied. (c) $G-V_{gs}$ characteristics. Panel a is converted into conductance, G. (d) I_{ds} vs V_{gs} and V_{ds} characteristics after irradiation of white light. (e) $I_{ds}-V_{ds}$ characteristic for various V_{gs} values from +10 to −10. $I_{ds}-V_{ds}$ curves become nonlinear when the gate voltages for a negative differential region are applied. (f) $G-V_{gs}$ characteristics under illumination. (g) Photo differential conductance.

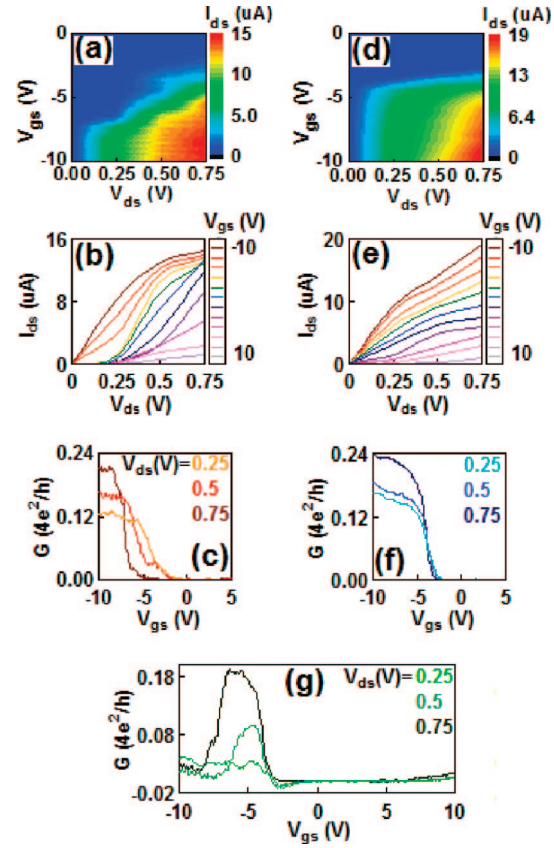

Figure 4. Electrical properties of Sample 2 before and after white light illumination. (a) I_{ds} vs V_{gs} and V_{ds} characteristics. (b) $I_{ds}-V_{ds}$ characteristic for various V_{gs} values from +10 to −10. (c) $G-V_{gs}$ characteristics. Panel a is converted into conductance, G. (d) I_{ds} vs V_{gs} and V_{ds} characteristics under white light illumination. Overall current was enhanced and the device became stable with less noise. (e) $I_{ds}-V_{ds}$ characteristic for various V_{gs} values from +10 to −10. $I_{ds}-V_{ds}$ curves become nonlinear when the gate voltages for a negative differential region are applied. (f) $G-V_{gs}$ characteristics under illumination. (g) Photo differential conductance.

V_{ds} values used. The differential photo conductance (DPC, the difference between conductance in the dark and under light illumination) was fluctuating rapidly within the first NDR range (Figure 3g).

Figure 4a shows a map of V_{gs} vs V_{ds} for nonilluminated intraconnect. Two negative differential resistance (NDR) regions are observed in the $I_{ds}-V_{gs}$ curve as well: one in the range between −3 and −6 V and another around −9 V (Figure 4b,c). The NDR peak for the first region was shifting albeit in both negative and positive directions as V_{ds} increased from 0.25 to 0.75 V. The second NDR region was stable around −9 V. The same intraconnect under white light illumination is shown in Figure 4d−f. Here, the light somewhat masked the NDR effect (Figure 3f) for the first V_{gs} region but left a small but noticeable presence around $V_{gs} \sim -9$ V. The DPC was stable and exhibited a marked increase for increasing V_{ds} (Figure 4g).

Discussion. NDR effect is the basis for many microwave oscillators.[27] The effect may be attributed to two competing transport venues, for example, nonlinear drift and thermionic venues or tunneling and thermionic excitation processes. In addition, optimal construction typically breaks the symmetry between the contact to and from the channel. For example, a CNT channel extending between two different metals,[13] which takes advantage of the metals' different work functions and the distribution of the tube's electronic density of states. In contrast, both of our electrodes were made of the same metal and hence we resorted to a gated configuration. The gate bias affects the distribution of carriers along the tube. If we postulate the existence of a secondary interface between the CNT channel and electrode, possibly in a form of a point Schottky contact or a quantum dot (QD), gate biasing affects the distribution of electronic states across such barrier, as well. We point to the very small, 1 nm thick catalytic seed film in our structures, which may result in a point contact during the tube's growth process. Tunneling may now occur between the tube and discrete states in this metal dot. The secondary NDR region for both samples may imply tunneling through a second QD band. Tunneling and transport must depend on the relative energy states' distribution between dot and channel, as well as, on the gate bias. NDR was also noted in our previous experiments while using another

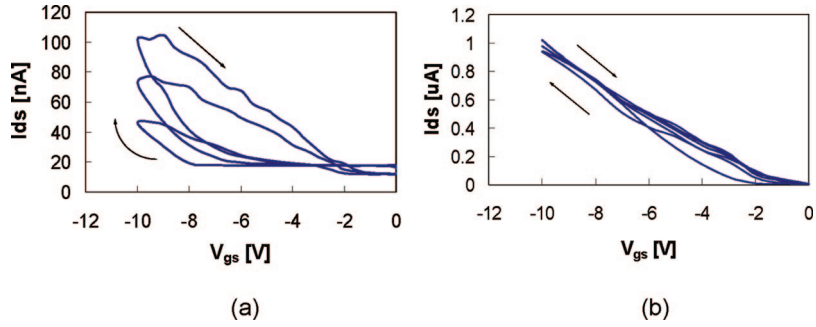

Figure 5. Hysteresis curves in the dark: (a) Nonlinear case, sample 1. (b) Linear case, sample 2. The arrows point the direction of the scan. In panel a, the overall current increased for increasing numbers of scans until stabilizing.

growth technique [ref 21, Figure 3] albeit at larger gate bias.

Sample 1 is probably made of individual or of a few tubes as judged by the narrow Raman RBM spectra; its current only weakly dependent on gate voltage and one may attribute its behavior to mostly the Schottky point interface. Its sensitivity to the contact with electrodes led to the asymmetry in the $I_{ds}-V_{ds}$ curve. In contrast, sample 2 is probably made of a small bundle thus is more likely to portray ohmic contact at zero gate bias. Sample 2 is more responsive to the gate bias as expected of a semiconductor channel.

Raman classification of the tubes may be distorted by stress and contact to the substrate.[26] In addition and despite careful alignment (see Supporting Information), the laser spot may cover tubes, which do not contribute to electrical conduction yet, may be at resonance with the laser line thus, affecting the Raman spectra. This could imply that both samples were of semiconductor type if we mainly base our conclusion on a self-consistent value for the tube's diameter. In that case, the samples differ only by the number of tubes in their respective bundles. Nevertheless, Raman spectroscopy is an important characterization tool, which corroborates the existence of nanotubes between electrodes and helps determine their type, thus complementing conductance measurements.

The characteristics of the channel under broadband optical excitation corroborated these findings, as well. Optical induced carriers in the channel overcame the tunneling process, hence the marked conductivity change for the first NDR region (around −5 V). The optical effect is smaller for the "nonlinear" sample 1 because of the interfering effect from the contact barrier. Moreover, since photoexcited carriers are composed of both types (holes and electrons), *n*-type characteristics at large positive gate voltages ought to be exhibited. Indications to such behavior are provided in Figure 4g. Furthermore, when the graphs are plotted as log plots (not shown) such characteristics are greatly accentuated. Both panels c and f of Figure 3 indicate a relatively sharp "ON" transition, which implies large channel mobility with back-to-back leaky Schottky diodes.[28] The ON transition in Figure 4c,f tends to have quadratic behavior as expected from an ordinary semiconducting channel.

Surface states play an important role in such devices. We observed hysteresis upon ramping the gate voltage in the negative and positive directions (Figure 5). The lower curves are always in the negative direction while the top curves are scanned from negative to positive gate bias values. The hysteresis did not change the presence of NDR which means that the latter is inherent to the tube/electrode contact but not to its surface. After a few scans, the hysteresis became narrower. This is to be expected of surface states. In addition, clockwise hysteresis is indicative of movable ions or, adsorbed water molecules (in contrast to charge trapped in the underlined oxide layer − the latter results in counter-clockwise hysteresis curve). Yet, sample 1 exhibited a large hysteresis and sample 2 exhibited almost a replica of the curve in the negative and positive gate bias ramp. That may be understood if the channel of sample 1 is composed of only few or even individual carbon nanotube. The effect of surface states must have been larger here than their effect on sample 2 with a larger bundle of tubes.

In summary, we demonstrated NDR in carbon nanotube gated structures under bias regardless of the linearity (or nonlinearity) of the contacts. The effect was accompanied by a large DPC. Since NDR enables the realization of microwave oscillators, one may envision that such DPC will be instrumental in designing new high-speed opto-electronic oscillators.

Supporting Information Available: This material is available free of charge via the Internet at http://pubs.acs.org.

References

(1) Wang, X.; Zhang, L.; Lu, Y.; Dai, H.; Kato, Y. K.; Pop, E. Electrically driven light emission from hot single-walled carbon nanotubes at various temperatures and ambient pressures. *Appl. Phys. Lett.* **2007**, *91*, 261102.

(2) Lu, Y.; Bangsaruntip, S.; Wang, X.; Zhang, L.; Nishi, Y.; Dai, H. DNA Functionalization of Carbon Nanotubes for Ultrathin Atomic Layer Deposition of High K Dielectrics for Nanotube Transistors with 60 mV/Decade Switching. *J. Am. Chem. Soc.* **2006**, *128*, 3518–3519.

(3) Kang, S. J.; Kocabas, C.; Ozel, T.; Shim, M.; Pimparkar, N.; Alam, M. A.; Rotkin, S. V.; Rogers, J. A. High-performance electronics using dense, perfectly aligned arrays of single-walled carbon nanotubes. *Nat. Nanotechnol.* **2007**, *2*, 230–236.

(4) Tans, S. J.; Devoret, M. H.; Dai, H.; Thess, A.; Smalley, R. E.; Geerligs, L. J.; Dekker, C. Individual single-wall carbon nanotubes as quantum wires. *Nature* **1997**, *386*, 474–477.

(5) Lu, W.; Lieber, C. M. Nanoelectronics from the bottom up. *Nat. Mater.* **2007**, *6*, 841–850.

(6) Rueckes, T.; Kim, K.; Joselevich, E.; Tseng, G. Y.; Cheung, C. L.; Lieber, C. M. Carbon Nanotube-Based Nonvolatile Random Access Memory for Molecular Computing. *Science* **2000**, *289*, 94–97.

(7) Lastella, S.; Mallick, G.; Woo, R.; Karna, S. P.; Rider, D. A.; Manners, L.; Jung, Y. J.; Ryu, C. Y.; Ajayan, P. M. Parallel arrays of individually addressable single-walled carbon nanotube field-effect transistors. *J. Appl. Phys.* **2006**, *99*, 24302.

(8) Kish, L. B.; Ajayan, P. M. Terrabyte flash memory with carbon nanotubes. *Appl. Phys. Lett.* **2005**, *86*, 93106.
(9) Bosnick, K.; Gabor, N.; McEuen, P. L. Transport in carbon nanotube p-i-n diodes. *Appl. Phys. Lett.* **2006**, *89*, 163121.
(10) Rosenblatt, S.; Yaish, Y; Park, J.; Gore, J.; Sazonova, V.; McEuen, P. L. High performance electrolyte gated carbon nanotube transistors. *Nano Lett.* **2002**, *2*, 869.
(11) Chen, Z.; Appenzeller, J.; Lin, Y.-M.; Sippel-Oakley, J.; Rinzler, A. G.; Tang, J.; Wind, S. J.; Solomon, P. M.; Avouris, P. An Integrated Logic Circuit Assembled on a Single Carbon Nanotube. *Science* **2006**, *311*, 1735.
(12) Léonard, F.; Tersoff, J. Multiple Functionality in Nanotube Transistors. *Phys. Rev. Lett.* **2002**, *88*, 258302.
(13) Léonard, F.; Tersoff, J. Negative Differential Resistance in Nanotube Devices. *Phys. Rev. Lett.* **2000**, *85*, 4767.
(14) Farajian, A. A.; Esfarjani, K.; Kawazoe, Y. Nonlinear Coherent Transport Through Doped Nanotube Junctions. *Phys. Rev. Lett.* **1999**, *92*, 5084.
(15) Zhou, C.; Kong, J.; Yenilmez, E.; Dai, H. Modulated Chemical Doping of Individual Carbon Nanotubes. *Science* **2000**, *290*, 1552.
(16) Yuzvinsky, T. D.; Mickelson, W.; Aloni, S.; Begtrup, G. E.; Kis, A.; Zettl, A. Shrinking a Carbon Nanotube. *Nano Lett* **2006**, *6*, 2718–2722.
(17) Iliea, A.; Egger, S.; Friedrichs, S.; Kang, D.-J.; Green, M. L. H. Correlated transport and high resolution transmission electron microscopy investigations on inorganic-filled single-walled carbon nanotubes showing negative differential resistance. *App. Phys. Lett.* **2007**, *91*, 253124.
(18) Li, X-F.; Chen, K.-Q.; Wang, L.; Long, M.-Q.; Zou, B. S.; Shuai, Z. Effect of length and size of heterojunction on the transport properties of carbon-nanotube devices. *App. Phys. Lett.* **2007**, *91*, 133511.
(19) Javey, A.; Guo, J.; Wang, Q.; Lundstrom, M.; Dai, H. Ballistic carbon nanotube field-effect transistors. *Nature* **2003**, *424*, 654.
(20) Heinze, S.; Tersoff, J.; Martel, R.; Derycke, V.; Appenzeller, J.; Avouris, P. Carbon Nanotubes as Schottky Barrier Transistors. *Phys. Rev. Lett.* **2002**, *89*, 106801.
(21) Katz, D.; Lopez, D.; Kornblit, A.; Grebel, H. Electrical and Optical Properties of Individual Carbon Nanotubes Bridging Addressable Metal Electrode Tips. *J. Nanosci. Nanotechnol.* **2008**, *8*, 1–5.
(22) Katz, D.; Lee, S.-W.; Lopez, D.; Kornblit, A.; Grebel, H. Synthesis of Carbon Nanotubes: Controlled Interconnects Growth. *J. Vac. Sci. and Tech., B* **2007**, *B25*, 1191.
(23) Kong, J.; Soh, H. T.; Cassell, A.; Quate, C. F.; Dai, H. Synthesis of Individual Single-Walled Carbon Nanotubes on Patterned Silicon Wafers. *Nature* **1998**, *395*, 878.
(24) Krupke, R.; Hennrich, F.; Lohneysen, H. V.; Kappes, M. M. Separation of Metallic from Semiconducting Single-walled Carbon Nanotubes. *Science* **2003**, *301*, 344–347.
(25) Jorio, A.; Filho, A. G. S.; Dresselhaus, G.; Dresselhaus, M. S.; Swan, A. K.; Unlu, M. S.; Goldberg, B. B.; Pimenta, M. A.; Hafner, J. H.; Lieber, C. M.; Saito, R. G-band resonant Raman study of 62 isolated single-wall carbon nanotubes. *Phys. Rev B* **2002**, *65*, 155412.
(26) Zhang, Y.; Son, H.; Zhang, J.; Dresselhaus, M. S.; Kong, J.; Liu, Z. Raman Spectra Variation of Partially Suspended Individual Single-Walled Carbon Nanotubes. *J. Phys. Chem. C.* **2007**, *111*, 1983–1987.
(27) Sze, S. M. *Physics of Semiconductor Devices*; Wiley-Interscience, New York, 1981.
(28) Lee, S. W., Grebel, H.; Kornblit, A.; Lopez, D. Electrical and optical properties of carbon nanotube/polypyrrole addressable intra-connects. *Synth. Met.* [Online early access]. DOI: 10.1016/j.synthmet.2008.11.015. Published online: January 11, 2009.

NL803036A